

Title	Sum-Frequency Generation and Scanning Electron Microscope Studies on Second-Harmonic Generation Active Structures of Sacran Aggregates
Author(s)	Phan, Thang Dinh; Mizutani, Goro; Li, Yanrong; Budpud, Kulisara; Okeyoshi, Kosuke; Okajima, Maiko; Kaneko, Tatsuo
Citation	e-Journal of Surface Science and Nanotechnology, 20: 98-106
Issue Date	2022-04-21
Type	Journal Article
Text version	publisher
URL	<a href="http://hdl.handle.net/10119/18025">http://hdl.handle.net/10119/18025</a>
Rights	Thang Dinh Phan, Goro Mizutani, Yanrong Li, Kulisara Budpud, Kosuke Okeyoshi, Maiko Okajima, Tatsuo Kaneko, e-Journal of Surface Science and Nanotechnology, 20, 2022, pp.98-106. DOI:/10.1380/ejssnt.2022-016. All articles published on e-J. Surf. Sci. Nanotechnol. are licensed under the Creative Commons Attribution 4.0 International (CC BY 4.0). You are free to copy and redistribute articles in any medium or format and also free to remix, transform, and build upon articles for any purpose (including a commercial use) as long as you give appropriate credit to the original source and provide a link to the Creative Commons (CC) license. If you modify the material, you must indicate changes in a proper way.
Description	



# Sum-Frequency Generation and Scanning Electron Microscope Studies on Second-Harmonic Generation Active Structures of Sacran Aggregates

Thang Dinh Phan, Goro Mizutani,<sup>†</sup> Yanrong Li, Kulisara Budpud, Kosuke Okeyoshi, Maiko Okajima, Tatsuo Kaneko

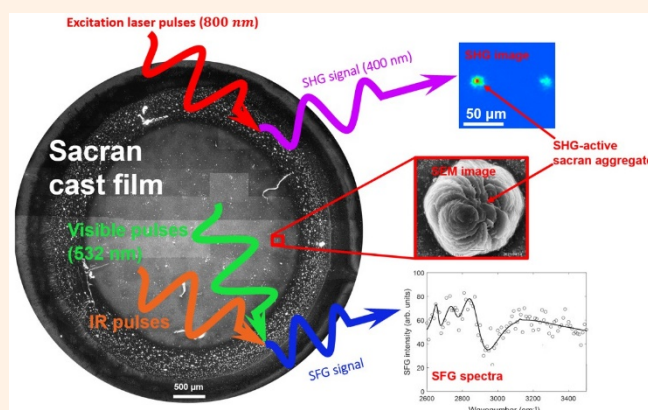
Japan Advanced Institute of Science and Technology, 1-1 Asahidai, Nomi, Ishikawa 923-1292, Japan

<sup>†</sup> Corresponding author: [mizutani@jaist.ac.jp](mailto:mizutani@jaist.ac.jp)

Received: 13 December, 2021; Accepted: 25 March, 2022; J-STAGE Advance Publication: 21 April, 2022; Published: 21 April, 2022

Optical second-harmonic generation (SHG) in self-assembled ampholytic mega-molecule polysaccharide sacran is an interesting phenomenon but its origin has not been clarified. SHG-active sacran aggregates in dried cast films made from ultrasonicated 0.5 wt% sacran aqueous solutions were studied at microscale using the scanning electron microscope and the energy dispersive X-ray technology. Hexagonal morphology was observed frequently with the size of a few to tens of micrometers. The calcium density was higher in the area showing the SHG signals. In sum-frequency generation spectra of the SHG-active sacran aggregates, vibrational modes of functional groups such as CH<sub>3</sub>, CH<sub>2</sub>, and –COOH of the sacran molecules and OH of the water molecules were identified. The structure of the SHG-active sacran aggregates was modeled from the observed facts.

**Keywords** Sacran; SHG microscopy; SFG spectroscopy; Scanning electron microscope (SEM); Energy-dispersive X-ray spectroscopy (EDS)



## I. INTRODUCTION

Polysaccharide sacran is an ampholytic mega-molecule (Figure 1) extracted from the cyanobacteria *Aphanothece sacrum* (*A. sacrum*) [1]. The molecular weight of sacran is  $M_w \approx 1.6 \times 10^7$  Da [2, 3] and it is much larger than that of other polymers such as cellulose ( $M_w \approx 20$ –150 kDa) [4] or xanthan gum ( $M_w \approx 4 \times 10^6$  Da) [5]. The polysaccharide sacran chain comprises various monosaccharides units as shown in Figure 1. Functional groups, such as carboxyl and sulfate, are the typical groups of sacran molecules and are used to distinguish polysaccharide sacran from other polysaccharides. Sacran has drawn great attention in applications such as pharmaceuticals, drugs, cosmetics, and food because of numerous sugar residues in its molecular structure [1, 2]. Fourier transform infrared spectroscopy shows the peak of

the carboxylate group at a wavenumber of  $1613 \text{ cm}^{-1}$ , while those of the sulfate group are at  $1223$  and  $1363 \text{ cm}^{-1}$  [6, 7]. The presence of the nitrogen element in the sacran chain demonstrated that sacran is an ampholytic sugar chain with an anion/cation ratio of about 30/1. The anions originate from the sulfate (~27%) and carboxylic (~22%) groups while cations are from amino sugars [2] (less than 1%).

Sacran molecules have ultrahigh absorbent capacity for water ( $6100 \text{ mL g}^{-1}$ ) and 0.9% saline ( $2700 \text{ mL g}^{-1}$ ) [8]. In the solution conditions, sacran is an amphoteric electrolyte material and sacran chains can change their conformation according to the concentration change. The spherical conformation was observed at a concentration  $< 0.004$  wt% [3]. The double helix and rigid structures formed at a concentration  $> 0.09$  wt% and changed to the soft filamentous structure at a concentration  $> 0.1$  wt% or the weak gel at a con-

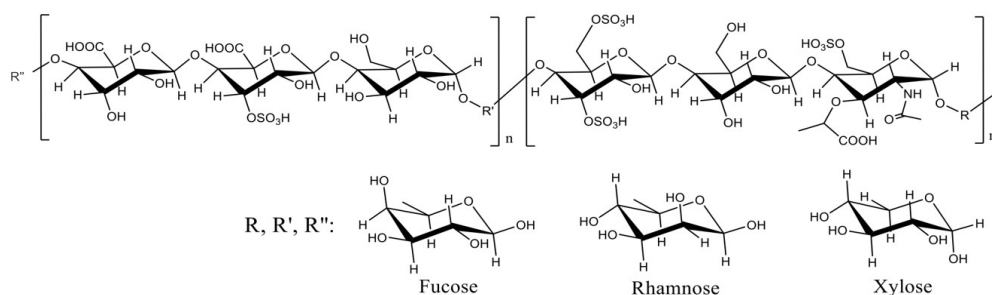


Figure 1: The partial structure of sacran.

centration > 0.25 wt%. This phase is characteristic of the increase in chain entanglement and fraction.

Sacran is in the nematic liquid crystallinity (LC) phase at a concentration of ~0.5 wt%. In the LC gel formation, sacran chains are aligned parallel to each other [3, 9]. The changing conformation of sacran chains in the solution conditions might be originated from the self-assembled ability of sacran chains [10]. Sacran cations and anions are thought to be the main factor in the self-assembly of the sacran aqueous solutions. The LC phase of sacran solutions can efficiently adsorb not only divalent but also trivalent metal ions, especially the rare earth metal ions [3, 11–16]. This is an interesting character of the sacran molecule and can be applied in bio-scavenger.

Sacran chains allow optical second-harmonic generation (SHG) phenomenon (Figure S1 in Supplementary Material) because of the chirality in their structure (Figure 1) [8], and the SHG spots in sacran cast films were observed by Zhao *et al.* [17, 18]. SHG is allowed for media with non-centrosymmetric structures at the molecular level [19–21]. SHG from macroscopic media is enhanced when the polarization of the constituent molecules is oriented in the same direction within the wavelength scale. According to Zhao *et al.*, the SHG signals from sacran molecules appear mostly as spots with sizes in the range from few to tens of micrometers, and it had a core part with the strongest intensity at the near center. Except for these spots most sacran molecules emit no SHG. The SHG intensity of the spots had an incident polarization dependence. Zhao *et al.* also detected SHG signals around a negative electrode of -4.5 V when the sacran aqueous solution was put in an electrode cell, applied voltage, and dried [18]. Hence, this SHG from the sacran films is not a trivial phenomenon, such as those from impurity or imperfection.

The origin of the SHG activity of sacran aggregates is mysterious and attracts our interest. This phenomenon is interesting not only as a property of sacran but also as a property of a general self-organizing polymer. Hence, in this study, our main purpose is to get more information about the SHG-active sacran aggregates to clarify the origin of the SHG activity. For this purpose, we modified sacran molecules and applied energy dispersive X-ray (EDX) and sum-frequency generation (SFG) methods. The original sacran solutions (0.5 wt%) were ultrasonicated, its molecular weight being made smaller by 20 to 80%, and then made

into cast films. Short-time ultrasonication was done because the SHG-active sacran becomes visible in linear images and becomes convenient for scanning electron microscopy (SEM) study. The number of SHG-active spots increased remarkably. SHG-active sacran aggregates are carefully and precisely positioned using the corresponding linear images and were observed by SEM and SEM-EDX. We found hexagonal structures with highly oriented subregions. Since these sacran aggregates should have a highly orientated structure and second-order optical nonlinearity, SFG spectra of dried sacran cast film were also studied. SFG spectra of SHG-active sacran aggregates showed vibrational modes of functional groups such as CH<sub>2</sub> or CH<sub>3</sub> and -COOH and a broadband from 3100 to 3400 cm<sup>-1</sup> of water molecules. Understanding the nonlinear second-order optical response of sacran molecules might lead to discovery of a high potential material that can be applied to telecommunications or optoelectronics industries in the future [22].

## II. MATERIALS AND EXPERIMENTS

### A. Sacran cast film preparation from ultrasonicated sacran aqueous solutions

The original sacran aqueous solutions (60 mL, 0.5 wt%) [1] were applied sonication with an ultrasonic tip 13 mm diameter made of a titanium alloy (Ti-6Al-4V) controlled by an ultrasonicator (SONICS Vibra cell VCX750, Sonics & Materials, a frequency of 20 kHz). The ultrasonication time was 10, 20, 30, and 40 s. The magnetic stirring was carried out during the ultrasonication process. This ensures that the entire sacran aqueous solution is exposed to the ultrasound probe, increasing the homogeneity needed for the entire sample. Ultrasonicated solutions had a 10-s cooldown time per every 50 s to avoid overheating. The ultrasonicated samples were centrifuged using centrifuge vaporizer equipment (EYELA CVE-200D) for 30–45 min to separate the metal fragments having a mass greater than the molecular weight of sacran molecules. To remove micro-scale dust particles possibly emitted from the irradiance probe of the sonic device, the syringe filter with a 5 μm of a pore size was used.

After the ultrasonic treatment, the molecular weight was a logarithmic function of a sonication energy. The sacran molecular weight decreased to less than one-third of their orig-

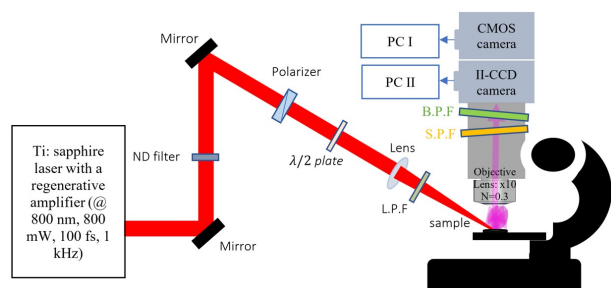


**Figure 2:** A schematic of the experimental setup for SHG observation. ND filter: neutral density filter, L.P.F.: long-pass filter (to remove light of wavelength shorter than 780 nm and pass the 800 nm beam), B.P.F.: bandpass filter (FF01-395/11 with transmittance over 90% at 388.4–402.2 nm and 92.9% at 400 nm), and S.P.F.: short-wavelength pass filter (passing 350–785 nm and rejecting 800 nm wavelength). A polarizer and a half-waveplate were used to set up the polarization of the incident laser light to investigate the polarization dependent SHG intensity.

inal weight after 30 s of ultrasonication as it is shown in Figure S2 (Supplementary Material). Viscosity of the sacran aqueous solution looked remarkably decreased [23]. Finally, ultrasonicated sacran aqueous solutions were dropped onto the surface of silicon substrates to form dried cast films at room temperature. Silicon wafers with native surface oxide layers were used as the substrates because they emit very weak SHG.

## B. Experiments

### 1. SHG and SFG experiments

**SHG experiment:** The experimental setup to determine the accurate position of the SHG-active aggregates in the cast films is shown in Figure 2, and detailed information about the experiment was described in our previous reports [17, 18]. Linear images of the sample were observed in the

same setup as the SHG observation above using white light illuminations and a complementary metal-oxide-semiconductor (CMOS) camera. SHG images were observed by using a bandpass filter of 400 nm wavelength and an image intensified charge-coupled device (II-CCD) camera with an accumulation time of 300 s. Two-photon excited fluorescence (2PEF) images (Figure S3 in Supplementary Material) were observed by using a bandpass filter of 438 nm wavelength and an II-CCD camera with an accumulation time of 60 s. The incident light wavelength was 800 nm, and the excitation power was 10 mW.

**SFG experiment:** The experimental setup for measuring the SFG spectra of sacran cast films can be also found in our previous report [24]. The fixed wavelength visible (Vis) light at 532 nm was laser pulses of time duration of 30 ps generated from a mode-locked Nd<sup>3+</sup>: YAG laser. The wave-number of the infrared (IR) light pulses generated from an optical parametric generator (OPG) was scanned in the range of 2600–3500 cm<sup>-1</sup>. The pulse energy of the visible light was set up at 80 μJ, and that of the IR pulse was about 150 μJ. The observation area was ~1 mm<sup>2</sup> on the film surface so it contained many SHG and SFG-active spots.

### 2. SEM and EDX-SEM experiments

SEM images of SHG-active sacran aggregates were observed using a NeoScope JCM-6000Plus, JEOL. For EDX-SEM analysis, we used TM3030Plus Miniscope-Hitachi. For high-resolution SEM images, dried cast films of sacran were coated with a gold layer of around 25 nm.

## III. RESULTS AND DISCUSSION

### A. SHG of selected sacran aggregates

Figure 3 shows optical linear, SHG, and 2PEF images of dried cast films made from original and ultrasonicated sacran solutions. In these figures, sacran is distributed all

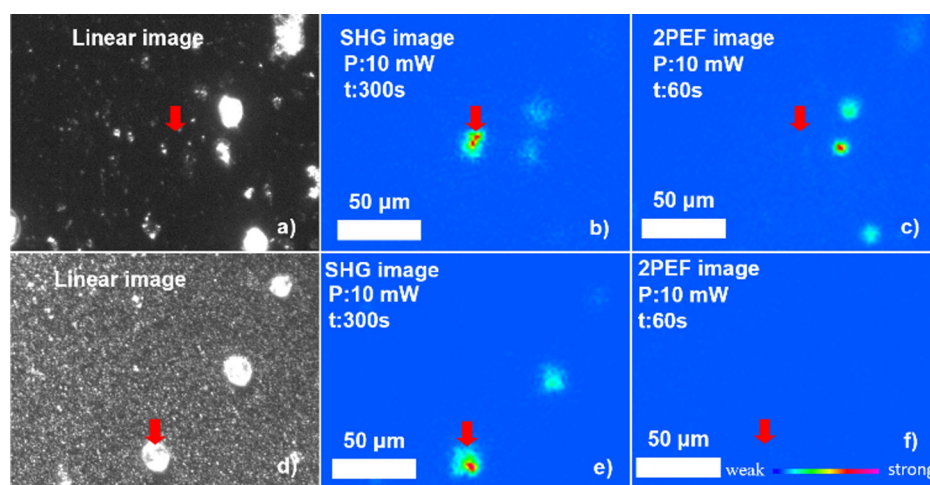


**Figure 3:** Linear, SHG, and 2PEF images (from left to right) observed from the sacran cast films made from the original sacran aqueous solution (a–c) and from the 30-s ultrasonicated sacran solutions (d–f). *P* and *t* represent excited laser power and integration time for image acquisition, respectively.

over the scopes of view. Yet, strong SHG signals in Figure 3(b, e) were observed only near the center region of the cast film. The red arrows mark the positions of the spotty SHG signals in the SHG images [Figure 3(b, e)]. We do not see any 2PEF signal at the red arrowed positions in Figure 3(c) or 3(f), and so we identified the spots in Figure 3(b, e) as SHG. If we see similar images at both 400 and 438 nm, the light at 400 nm can be from a tail of 2PEF. In the linear image of the film made from the original sacran solution [Figure 3(a)], nothing is seen at the position indicated by the red arrow. This is the reason why we could not try to see SEM images of this sample. On the other hand, in the linear image of the film made from the sonicated sacran solution [Figure 3(d)], a clear spot is seen at the position indicated by the red arrow. Hence, we did SEM observation of this sample as in the next section. The SHG active aggregates in the film made from the sonicated sacran solution have the size of a few to 20  $\mu\text{m}$  in the linear image.

In the case of 10 s of the ultrasonicated sacran aqueous solution, the SHG signals appeared with more complex shapes such as rod-shaped or with quite uniform intensity between the center and edge regions. The SHG intensity decreased significantly at the ultrasonication times longer than 40 s.

## B. The hexagonal structure of SHG-active sacran aggregates

Figures 4 are linear, SEM, SHG, and 2PEF images of SHG-active sacran aggregates of ultrasonicated sacran solution of 20 s [Figure 4(a–d)] and 30 s [Figure 4(e–h)]. Figures 4(a, c, d) and 4(e, g, h) as groups are shown on the same scale, and Figures 4(b) and 4(f) are expanded. In the linear image of Figure 4(a) we see a particle with a diameter of 13  $\mu\text{m}$ , although its contrast is not uniform. The SEM image shows some multilayer symmetric structures with different diameters. In the SHG image of Figure 4(c), we see two spots. The left spot has an intense peak at its center and its position is indicated by a white arrow. Figure 4(g) shows

a spot with higher intensity at the near center of the spot. In the 2PEF images in Figure 4(d, h), almost nothing is seen. Sacran sometimes gives both SHG and 2PEF as in Figure 4(g, h). However, the 2PEF intensity in Figure 4(h) is much weaker than the SHG intensity [Figure 4(g)] and has a broad distribution instead of a sharp peak [Figure S4(d) in Supplementary Material]. The power dependence of the SHG signal was a quadratic function [Figure S4(e)]. Multi-photon fluorescence was investigated by using a band pass filter of 370- and 390-nm wavelengths and no signal was seen at all [Figure S4(h, k)]. Hence, there is no three or four photon-excited fluorescence under the current excitation power. These indicate that the signal detected in Figure 4(c, g) are SHG.

SEM images in Figure 4(b, f) are observed frequently for ultrasonicated sacran solutions. The shape of the particle in Figure 4(b) looks roughly hexagonal. Typical images of hexagonal structures are seen in Figure 5(a, c, e, g), besides some other complex-shaped structures in Figure 5(b, d, f, h), among the SHG active spots of the ultrasonicated sacran aqueous solutions of 10, 20, 30, and 40 s. In Figure 5(a) at 10 s of the ultrasonication time (an input energy of 7.2  $\text{kJ mL}^{-1}$ ), fibrous sacran is seen in the edge region of the hexagonal particle [10, 25–28]. Microdomains, forming layer-like structures are arranged frequently around some centers, most typically holes as seen in Figure 5(a, b, f, g) [23, 25, 29]. Nanofiber sacran structures disappeared at higher ultrasonic energies than 12.2  $\text{kJ mL}^{-1}$  (20 s of the ultrasonication time). When the ultrasonication times are 10, 20, and 30 s, hexagonal particles like those in Figure 5(a, c, e) appear prominently on the surface of the sacran cast film. With higher ultrasonic energy ( $\sim 24 \text{ kJ mL}^{-1}$ ), many smaller particles with submicron sizes appear on the surface [Figure 5(g, h)], and there were no hexagonal-shaped SHG-active aggregates.

These hexagonal structures are rather two-dimensional (2D) particles or of pancake shapes of roughly  $D_{6h}$  symmetry and the central holes look like the symmetry axes in Figure 5(a, b, e–g). In addition, in Figure 5(d) the particle

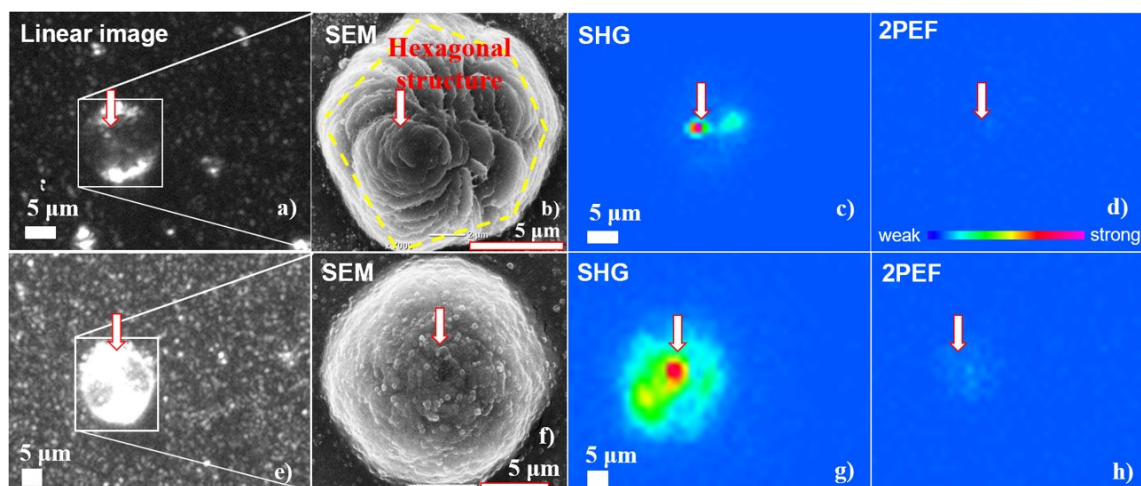
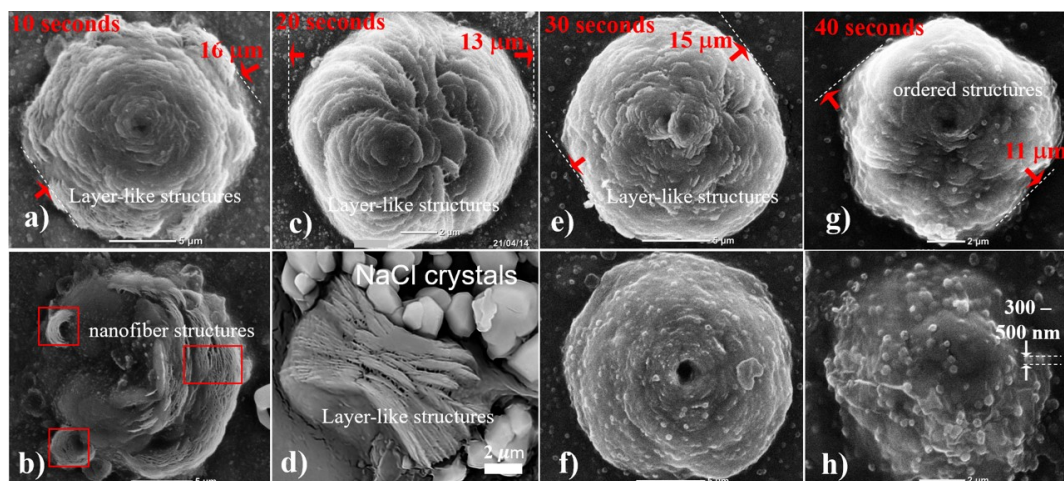


Figure 4: Linear, SEM, SHG, and 2PEF images of SHG-active sacran aggregates with the sizes of 13  $\mu\text{m}$  (b) and 15  $\mu\text{m}$  (f).



**Figure 5:** SEM images of hexagonal and highly ordered structures of the SHG-active sacran aggregates in the cast films made from the sacran aqueous solutions of ultrasonication times of (a, b) 10 s, (c, d) 20 s, (e, f) 30 s, and (g, h) 40 s.

appears to have shrunk into a 2D sheet when water was removed by drying, so its thickness is suggested to be thin.

The bottom row of **Figure 5** shows some SHG-active sacran particles with complicated shapes in SEM images. The white polyhedral structures in **Figure 5(d)** are believed to be NaCl crystals since chemical element analysis in **Figure S5 (Supplementary Material)** showed Na species.

To examine the constituent chemical elements of the SHG-active hexagonal sacran aggregate in **Figure 5(c)**, we show its EDX-SEM element map in **Figure 6**. The four elements C, O, S, and N are major elements making up sulfate, carboxyl, and amide groups in sacran. In particular, the existence of element S proves that the SHG-active hexagonal structures are sacran aggregates. EDX-SEM results of aggregates from other ultrasonicated sacran solutions were similar.

From **Figure 6**, atomic percentage ratios ( $r$ ) of Na and Ca to S, defined as

$$r_{\text{Na,Ca/S}} = \frac{\text{Atomic \% of Na or Ca}}{\text{Atomic \% of S}}$$

were obtained. We found that the areas without SHG signals had the ratio  $r_{\text{Ca/S}} < 1$ , while that with SHG-active spot had a ratio larger than 4 ( $r_{\text{Ca/S}} > 4$ ). Those ratios for the Na element ( $r_{\text{Na/S}} = 4\text{--}8$ ) were roughly uniform in all the areas.

Zhao *et al.* observed a strong anisotropy of SHG spots as a function of the incident polarization angle in a film made from unsonicated sacran aqueous solution [17]. In the same way, we carried out a polarization-dependent SHG experiment on a hexagonal SHG-active sacran aggregate (**Figure S6 in Supplementary Material**). The polarization angle of incident light was defined as  $\theta = 0^\circ$  when it was p-polarized after a polarizer [**Figure 7(a)**]. The output SHG polarization was not specified. The SHG intensity as a function of  $\theta$  is shown in **Figure 7(b)** in red and black dots for (1) and (2) sample configurations, respectively.

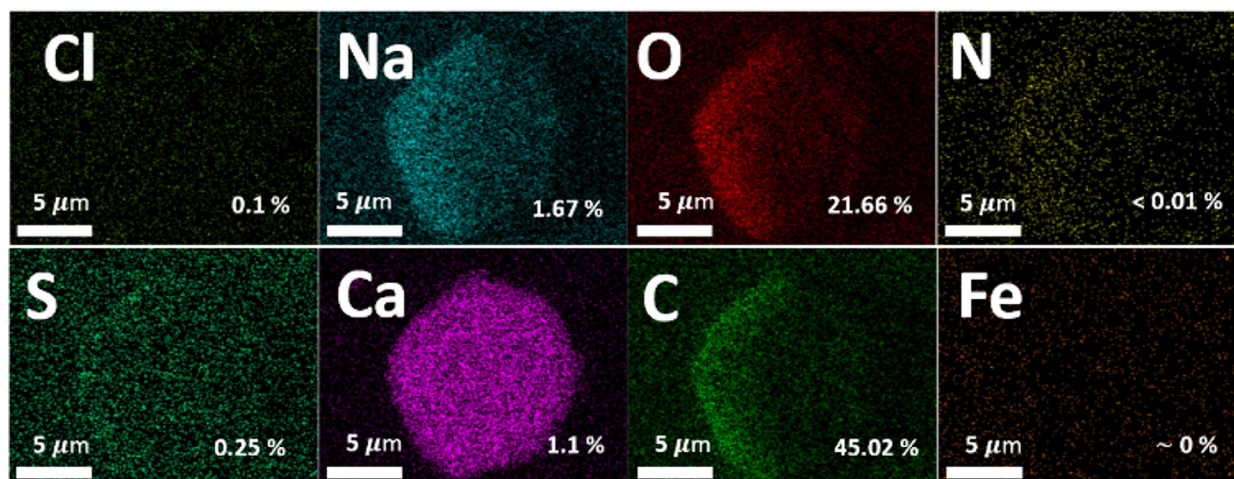


**Figure 6:** Maps showing the chemical elements in a sacran aggregate shown in **Figure 5(c)** by using EDX-SEM technique.

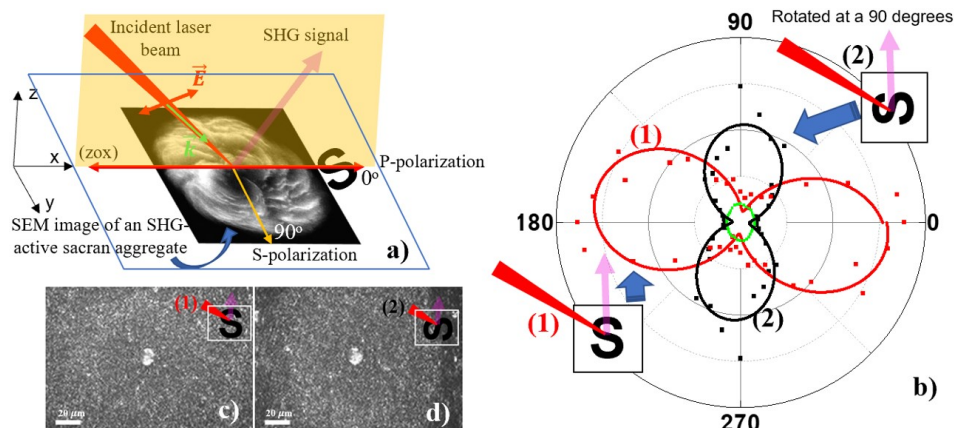


**Figure 7:** (a) Polarization of incident laser beam for  $\theta = 0^\circ$  (p-polarization), (b) the polarization-dependent SHG intensity of the SHG-active sacran aggregates. Red and black dots and curves labeled (1) and (2), respectively, are data for the samples in two different configurations shown at the edges. The green square dots are 2PEF intensity. (c, d) S-polarized linear images corresponding to the (1) and (2) cases.

In Figure 7(b), the red and black curves are fitting data using the formulation [30]:

$$I_{\text{SHG}} \propto a[(\sin^2\theta + b \cos^2\theta)^2 + c \sin^2\theta \cos^2\theta]$$

Here  $a$ ,  $b$ , and  $c$  are constants related to the third-rank tensor of the second-order nonlinear susceptibility  $\chi^{(2)}$ . One can see in Figure 7(b) that the SHG intensity pattern is clearly anisotropic and that it rotates according as the sample is rotated. The reason for the different maximum intensity between (1) and (2) patterns is the difference of Fresnel factors when the incident electric field is in the optimum SHG emitting direction of the aggregate. The 2PEF intensity shown in green in Figure 7(b) has a circular shape as a function of the incident polarization angle and is much weaker than the SHG intensities. S-polarized linear images of the same SHG-active aggregate using a white light as a function of the sample rotational angle around its surface normal are shown in Figure 7(c, d). More detailed sample rotation angle dependence is shown in Figure S6 (Supplementary Material). The last two results show that the aggregates appear to be isotropic in the linear optical and 2PEF phenomena.

### C. The SFG spectra

We obtained SFG spectra of dried sacran cast films made from 20-s ultrasonicated sacran solutions (the ultrasonic energy of  $12.2 \text{ kJ mL}^{-1}$ ; Figure S7 in Supplementary Material), as shown in Figure 8. Here we note that the cast films with no ultrasonic treatment show very weak SFG. We observed SFG spectra from two different regions of the sacran cast film; the first is the edge region and the second is near the center. The edge region has a very high spotty SHG density ( $176.23 \text{ spots mm}^{-2}$ ). This region should have a high second-order nonlinearity, and this is the reason why we chose it for the SFG measurement. The density of SHG spots near the center ( $24.5 \text{ spots mm}^{-2}$ ) was much less than that of the edge region. Accordingly, we have a clear SFG spectrum for the edge region [Figure 8(a)], while only a

noise signal was detected near the center [Figure 8(c)].

In Figure 8(a, b), red and green fitting curves were drawn by using the equation [31]:

$$S(\omega_{\text{SFG}}) \propto \left| \bar{\chi}_{\text{NR}}^{(2)} + \sum_n \frac{\vec{A}_n \exp(i\theta_n)}{\omega_{\text{IR}} - \omega_n + i\Gamma_n} \right|^2$$

Here,  $\bar{\chi}_{\text{NR}}^{(2)}$ ,  $n$ ,  $\omega_n$ ,  $\omega_{\text{IR}}$ ,  $\vec{A}_n$ , and  $\Gamma_n$  are the non-resonant background in  $\bar{\chi}^{(2)}$ , the order of resonance, the frequency of the  $n$ th resonance, the frequency of IR light, the amplitude, and the damping coefficient of the  $n$ th vibrational mode, respectively. In the red curve, the peak at around  $2850 \text{ cm}^{-1}$  is assigned to the symmetric stretching mode of  $\text{CH}_3$  or  $\text{CH}_2$

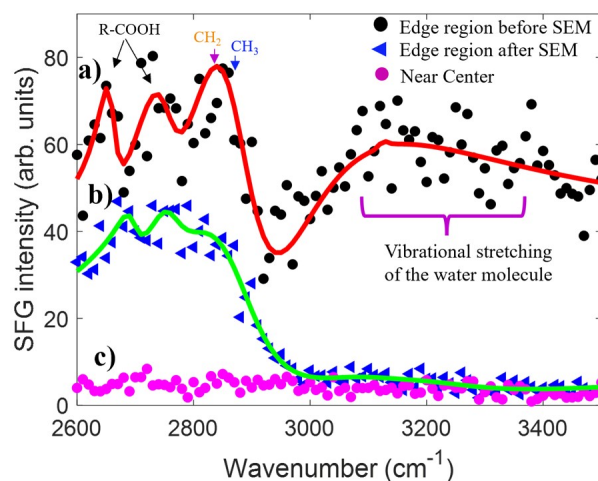


**Figure 8:** SFG spectra of a dried cast film made from the 20-s ultrasonicated sacran solution. (a) Black dots and the red curve are measured SFG data and a fitting curve at the edge region of the cast film, respectively. (b) Blue triangles and the green curve are measured SFG data and a fitting curve at the edge region of the cast film, respectively, after it was kept in a vacuum for 2 h. (c) Red dots are measured SFG intensity near the center of the cast film before the film was kept in a vacuum.

[6, 7, 32] and the peak at 2650 and  $\sim 2750\text{ cm}^{-1}$  are assigned to the OH stretching mode of the R-COOH group [6]. The broadband from 3100 to  $3400\text{ cm}^{-1}$  is assigned to the vibrational OH stretching mode of water. This water band is not seen in the SFG spectra of the cast film kept in a vacuum for 2 h [Figure 8(b)]. The water molecules would have been removed from the film in the vacuum.

#### D. Modeling of SHG-active sacran aggregates

Based on the results in Sections III.A–III.C, we will suggest a model structure of the SHG-active sacran aggregates. For this purpose, we first summarize below the facts found out in the previous sections:

- (1) SHG-active sacran aggregates became visible in linear images after ultrasonication treatment of the source sacran aqueous solution, while it was not before the treatment.
- (2) The number of SHG spots increased after ultrasonication treatment up to 20 s ( $12.2\text{ kJ mL}^{-1}$ ) and decreased for a longer sonication time.
- (3) Hexagonal structures were observed in many of the SEM images of SHG active spots in the cast film made from the 10- to 40-s ultrasonicated sacran aqueous solutions.
- (4) In the hexagonal structure, Na, O, S, Ca, and C elements are uniformly distributed. The Ca to S ratio in the SHG-active region is four-time higher than that in the non-SHG-active region.
- (5) SFG spectra were observed for cast films made from sacran aqueous solutions ultrasonicated for 20 s.
- (6)  $\text{CH}_2$  and  $\text{CH}_3$  related peaks, R-COOH peaks, and a water peak were observed in the SFG spectra
- (7) The water SFG peak disappeared after the cast film was evacuated.

Next, we list up some of the properties of SHG active spots found in literature [17, 18]:

- (8) Most SHG signals have spotty shapes and have a very strong intensity near the center of the spots.
- (9) SHG images of the SHG-active sacran aggregates consist of concentric multilayer structures.
- (10) The SHG intensity spots have a strong incident polarization dependence but the 2PEF intensity does not.
- (11) When a sacran aqueous solution is put in an electrode cell and applied an electric voltage of 4.5 V and a current until it dries, SHG of sacran film becomes active near the negative electrode [18].
- (12) All the sacran molecules take rod-like structures with diameter of several micrometers and length larger than  $200\text{ }\mu\text{m}$  above a threshold concentration and show a liquid crystal phase [10, 25, 28, 33].

Figure 9 is our proposed tentative model structure of the SHG-active sacran aggregates. In the center of the SHG-active region, there might be positively charged sacran chains, because, according to property (11), the existence of positively charged sacran molecules is suggested [17, 18]. In Figure 9, we show only the charges and no sacran molecules.

These positively charged sacran chains are minority species, but they attract negatively charged sacran chains and form a central electric dipole. Other dipoles created around this central dipole are drawn as empty arrows. They are oriented in the same direction as each other and make a macroscopic dipole according to property (10). Outside the SHG spot, there are random dipoles created by the sacran molecules. They make no macroscopic dipole. Within the SHG spot, we show the water molecules. These water molecules are aligned in the same direction as each other so that the SFG of these water molecules are active according to properties (6) and (7).

From property (10), permanent dipoles of sacran molecules' aggregates' are suggested to be aligned in one direction. Property (5) supports this view because such an anisotropy induces SFG activity of sacran molecules. In Figure 7(b), the SHG pattern as a function of the polarization angle rotates by  $90^\circ$  when the sample is rotated by  $90^\circ$ . This confirms that permanent dipoles of sacran molecules' aggregates are aligned in one direction as shown in Figure 9.

The driving force of the alignment of the dipoles of sacran molecules is not yet clearly understood. There are three possible candidates for the origin of such forces. The first one is a branching of sacran molecules like that in amylopectin. Amylopectin and amylose in starch are composed of  $\alpha$ -D-glucose polymer with  $\alpha$ -(1,4) glycosidic bonds. Amylopectin is SHG and SFG active because all the reducing ends are oriented in the same direction by the effect of the branching by  $\alpha$ -(1,6) glycosidic bonds. Amylose is SHG and SFG inactive because the saccharide chains have their reducing ends up and down by 50% each and the nonlinear polarization cancels. It is a probable candidate because it has been pointed out that multi-valent metal ions (like Ca in this paper) bind with carboxylate and sulfate groups in the sacran chain and serve as crosslinkers of different chains [10]. However, the reason why there are two kinds of bundle structures with and without macroscopic dipole is not known yet.

The second candidate is a Coulomb force induced by the central cation. If the positive charge of the central cation is large it creates a Coulomb potential, and the potential will

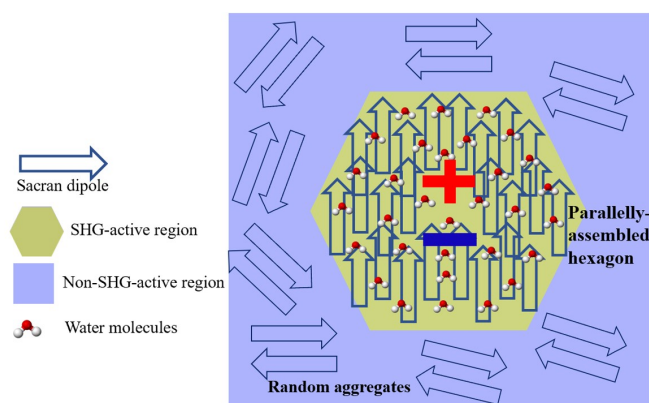


Figure 9: Plausible model of SHG-active sacran dipole aggregates.

align the sacran molecules and their dipoles. However, this candidate has a problem that it does not explain the uni-directional alignment of the dipoles in the SHG spot.

The third candidate is a possible ferroelectric liquid crystal phase of sacran molecules. Sacran has abundant chiral units giving possible structures to form a ferroelectric liquid crystal (FLC) [34, 35]. Permanent electric dipoles of the sacran chain can occur if the chain takes a spiral structure by the effect of the alternate alignment between non-chiral and chiral molecules. This random organization of the molecules creates a layer dipole moment, and a helicoidal structure of chiral smectic C (SmC\*) liquid crystal ferroelectric phase [36]. As another ferroelectric liquid crystal phase, a splay nematic phase is also reported. [37–39].

The nonzero SFG signal of water molecules mentioned in property (5) shows that the water molecules are oriented also. This may be caused by the orientation of the dipoles of the sacran molecules and the fact endorses the assumption that the dipoles of the sacran molecules are oriented.

A uniform distribution of sodium and calcium cations in the sacran aggregates in property (4) suggests that the distribution of chemical elements is uniform in spite of the fact that the SHG intensity has a small and sharp core at the center. The mechanism of the correlation of the SHG activity and Ca density is not understood.

In the SHG-inactive region, there might be a cancellation of electric dipoles of a pair of sacran molecules. This model is suggested according to the analogy with SHG and SFG activities of amylose and amylopectin as we have stated above. If the reducing ends of sacran chains are up and down by 50% each, the SHG and SFG will be inactive.

The hexagonal structures as they can be seen in Figure 5 have not been reported so far. No information is available on what the microscopic origin of this morphology is. However, it is interesting to guess the relationship between this structure and properties (4) and (6). These two properties clearly show that water is contained in the SHG active aggregates as shown in Figure 5. In addition, as already suggested above, water is well aligned in the aggregates as illustrated in Figure 9. Hence the hexagonal shape might come from an ice crystalline morphology like that of a snowflake. This hypothesis may be strange because our samples are kept at room temperature. However, as pointed out by Shen *et al.*, water is said to have an ice structure in a significant part even above the melting point [30] so that water can lead to the observed hexagonal structure. If this is the case, the SHG activity and the hexagonal structure of the SHG-active aggregates may be correlated because they are both induced by the dipole generation in the sacran cast film. An alternative origin of the hexagonal structure can be crystalline phases containing hexagonal spiral structures of saccharide chains such as those of amylopectin [40].

## IV. CONCLUSIONS

In this study, SHG-active sacran aggregate structures in the cast film made from ultrasonicated sacran aqueous solu-

tion were analyzed by combining the SHG microscope, SEM/EDX-SEM, and SFG techniques. The SHG signals appeared most frequently in a spotty shape with high intensity near the center. According to the SEM images, the SHG-active sacran aggregates can self-assemble to a hexagonal structure of sizes of several to 20  $\mu\text{m}$  having extremely high oriented and concentric multilayer-like structure units. The presence of counter cations of sodium and calcium with a high uniform distribution was confirmed as it is consistent with the efficient metal ion absorption properties. The calcium density is higher in the area showing the SHG signals. The SFG spectra were observed from the area with a higher number density of the SHG spots in the film. The SFG spectra show peaks of vibrational modes of functional groups such as  $\text{CH}_3$ ,  $\text{CH}_2$ ,  $\text{COOH}$ , and a broadband of an O–H stretching mode of water. In our tentative model of the SHG-active sacran aggregate, the SHG phenomenon originates from the main electric dipole at the center created by positively and negatively charged sacran, with well-oriented dipoles induced by the sacran chains in the surrounding area.

## Appendix

Illustration of the SHG and 2PEF phenomena, the measured molecular weight of sacran as a function of the ultrasonication energy, an incident power dependence of the SHG intensity, SEM and multi-photon excited fluorescence images, chemical mapping images by EDS, an angle dependence of linear images under s-polarized white light illumination, various types of SHG-active sacran aggregates, and a schematic SHG image of a whole sacran cast film are available in Supplementary Material at <https://doi.org/10.1380/ejsnt.2022-016>.

## Note

This paper was presented at the 13th International Symposium on Atomic Level Characterizations for New Materials and Devices '21 held online (ALC '21 Online), October 19 & 20, 2021.

## References

- [1] M. Okajima-Kaneko, M. Ono, K. Kabata, and T. Kaneko, *Pure Appl. Chem.* **79**, 2039 (2007).
- [2] M. K. Okajima, T. Bamba, Y. Kaneko, K. Hirata, E. Fukusaki, S. Kajiyama, and T. Kaneko, *Macromolecules* **41**, 4061 (2008).
- [3] T. Mitsumata, T. Miura, N. Takahashi, M. Kawai, M. K. Okajima, and T. Kaneko, *Phys. Rev. E* **87**, 042607 (2013).
- [4] T. Dürig and K. Karan, in: *Handbook of Pharmaceutical Wet Granulation: Theory and Practice in a Quality by Design Paradigm*, edited by A. S. Narang and S. I. F. Badawy (Academic Press, 2019) pp. 317–349.
- [5] G. Holzwarth, *Carbohydr. Res.* **66**, 173 (1978).
- [6] P. J. Larkin, *Infrared and Raman Spectroscopy: Principles and Spectral Interpretation* (Elsevier, 2011).
- [7] B. H. Stuart, *Infrared Spectroscopy: Fundamentals and Applications* (John Wiley & Sons, 2004).
- [8] M. K. Okajima, T. Bamba, Y. Kaneko, K. Hirata, E. Fukusaki, S. Kajiyama, and T. Kaneko, *Macromolecules* **41**, 4061 (2008).

- [9] M. K. Okajima, D. Kaneko, T. Mitsumata, T. Kaneko, and J. Watanabe, *Macromolecules* **42**, 3057 (2009).
- [10] K. Budpud, K. Okeyoshi, M. K. Okajima, and T. Kaneko, *Small* **16**, 2001993 (2020).
- [11] M. K. Okajima, S. Miyazato, and T. Kaneko, *Langmuir* **25**, 8526 (2009).
- [12] M. K. Okajima, M. Nakamura, T. Mitsumata, and T. Kaneko, *Biomacromolecules* **11**, 1773 (2010).
- [13] Q. T. le Nguyen, M. Okajima, T. Mitsumata, K. Kan, H. T. Tran, and T. Kaneko, *Colloid Polym. Sci.* **290**, 163 (2011).
- [14] M. K. Okajima, T. Higashi, R. Asakawa, T. Mitsumata, D. Kaneko, T. Kaneko, T. Ogawa, H. Kurata, and S. Isoda, *Biomacromolecules* **11**, 3172 (2010).
- [15] T. Kaneko, M. Okajima, and S. Tateyama, *Nippon Gomu Kyokaishi* **87**, 146 (2014) (in Japanese).
- [16] M. K. Okajima, Q. T. le Nguyen, M. Nakamura, T. Ogawa, H. Kurata, and T. Kaneko, *J. Appl. Polym. Sci.* **128**, 676 (2013).
- [17] Y. Zhao, K. T. T. Hien, G. Mizutani, H. N. Rutt, K. Amornwachirabodee, M. Okajima, and T. Kaneko, *J. Opt. Soc. Am. A* **34**, 146 (2017).
- [18] Y. Zhao, Y. Li, K. T. T. Hien, G. Mizutani, N. Ito, H. N. Rutt, M. Okajima, and T. Kaneko, *J. Phys. Soc. Japan* **86**, 124401 (2017).
- [19] R. W. Boyd, *Nonlinear Optics* (Academic Press, 2008).
- [20] N. Bloembergen, *Nonlinear Optics* (Benjamin, New York, 1965).
- [21] W. Chen, M. B. Feller, and Y. R. Shen, *Phys. Rev. Lett.* **63**, 2665 (1989).
- [22] J. M. Cole, *Philos. Trans. Royal Soc. A* **361**, 2751 (2003).
- [23] M. K. Okajima, R. Mishima, K. Amornwachirabodee, T. Mitsumata, K. Okeyoshi, and T. Kaneko, *RSC Adv.* **5**, 86723 (2015).
- [24] H. C. Hieu, H. Li, Y. Miyauchi, G. Mizutani, N. Fujita, and Y. Nakamura, *Spectrochim. Acta A* **138**, 834 (2015).
- [25] K. Okeyoshi, M. K. Okajima, and T. Kaneko, *Polym. J.* **53**, 81 (2021).
- [26] K. Okeyoshi, M. K. Okajima, and T. Kaneko, *Sci. Rep.* **7**, 5615 (2017).
- [27] K. Okeyoshi, T. Shinhama, K. Budpud, G. Joshi, M. K. Okajima, and T. Kaneko, *Langmuir* **34**, 13965 (2018).
- [28] K. Okeyoshi, M. K. Okajima, and T. Kaneko, *Biomacromolecules* **17**, 2096 (2016).
- [29] G. Joshi, K. Okeyoshi, M. K. Okajima, and T. Kaneko, *Soft Matter* **12**, 5515 (2016).
- [30] D. S. James and P. J. Campagnola, *BME Front.* **2021**, 3973857 (2021).
- [31] Y. R. Shen and V. Ostroverkhov, *Chem. Rev.* **106**, 1140 (2006).
- [32] D. Lin-Vien, W. G. Fateley, N. B. Colthup, and J. G. Grasselli, *The Handbook of Infrared and Raman Characteristic Frequencies of Organic Molecules* (Academic Press, 1991).
- [33] K. Shikinaka, K. Okeyoshi, H. Masunaga, M. K. Okajima, and T. Kaneko, *Polymer* **99**, 767 (2016).
- [34] A. Seki, M. Yoshio, Y. Mori, and M. Funahashi, *ACS Appl. Mater. Interfaces* **12**, 53029 (2020).
- [35] K. Skarp and M. A. Handschy, *Mol. Cryst. Liq. Cryst. Inc. Nonlinear Opt.* **165**, 439 (1988).
- [36] S. Pirkel and M. Glogarova, in: *Ferroelectrics—Physical Effects*, edited by M. Lallart (IntechOpen, 2011) Chap. 17.
- [37] A. Mertelj, L. Cmok, N. Sebastián, R. J. Mandle, R. R. Parker, A. C. Whitwood, J. W. Goodby, and M. Čopič, *Phys. Rev. X* **8**, 041025 (2018).
- [38] R. J. Mandle and A. Mertelj, *Phys. Chem. Chem. Phys.* **21**, 18769 (2019).
- [39] N. Sebastián, L. Cmok, R. J. Mandle, M. R. de la Fuente, I. Drevnšek Olenik, M. Čopič, and A. Mertelj, *Phys. Rev. Lett.* **124**, 037801 (2020).
- [40] L. Kong, C. Lee, S. H. Kim, and G. R. Ziegler, *J. Phys. Chem. B* **118**, 1775 (2014).



All articles published on e-J. Surf. Sci. Nanotechnol. are licensed under the Creative Commons Attribution 4.0 International (CC BY 4.0). You are free to copy and redistribute articles in any medium or format and also free to remix, transform, and build upon articles for any purpose (including a commercial use) as long as you give appropriate credit to the original source and provide a link to the Creative Commons (CC) license. If you modify the material, you must indicate changes in a proper way.

Copyright: ©2022 The author(s)

Published by The Japan Society of Vacuum and Surface Science